

# Experimental and theoretical studies of charge transfer and deuterium ion transfer between $D_2O^+$ and $C_2H_4$

Li Liu, Xiaohui Cai, Yue Li, Elizabeth Richards O'Grady, and James M. Farrar<sup>a)</sup>  
*Department of Chemistry, University of Rochester, Rochester, New York 14627*

(Received 12 March 2004; accepted 20 May 2004)

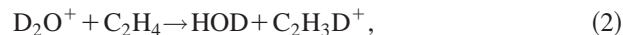
The charge transfer and deuterium ion transfer reactions between  $D_2O^+$  and  $C_2H_4$  have been studied using the crossed beam technique at relative collision energies below one electron volt and by density functional theory (DFT) calculations. Both direct and rearrangement charge transfer processes are observed, forming  $C_2H_4^+$  and  $C_2H_3D^+$ , respectively. Independent of collision energy, deuterium ion transfer accounts for approximately 20% of the reactive collisions. Between 22 and 36% of charge transfer collisions occur with rearrangement. In both charge transfer processes, comparison of the internal energy distributions of products with the photoelectron spectrum of  $C_2H_4$  shows that Franck-Condon factors determine energy disposal in these channels. DFT calculations provide evidence for transient intermediates that undergo H/D migration with rearrangement, but with minimal modification of the product energy distributions determined by long range electron transfer. The cross section for charge transfer with rearrangement is approximately  $10^3$  larger than predicted from the Rice-Ramsperger-Kassel-Marcus isomerization rate in transient complexes, suggesting a nonstatistical mechanism for H/D exchange. DFT calculations suggest that reactive trajectories for deuterium ion transfer follow a pathway in which a deuterium atom from  $D_2O^+$  approaches the  $\pi$ -cloud of ethylene along the perpendicular bisector of the C–C bond. The product kinetic energy distributions exhibit structure consistent with vibrational motion of the D-atom in the bridged  $C_2H_4D^+$  product perpendicular to the C–C bond. The reaction quantitatively transforms the reaction exothermicity into internal excitation of the products, consistent with mixed energy release in which the deuterium ion is transferred in a configuration in which both the breaking and the forming bonds are extended. © 2004 American Institute of Physics. [DOI: 10.1063/1.1772365]

## I. INTRODUCTION

The processes of charge transfer and proton transfer are two of the most common reactions that occur in gas phase ion chemistry.<sup>1,2</sup> Studies of such processes under single collision conditions yield insight into their reaction dynamics in a manner that provides incisive tests of theoretical treatments of the potential energy surfaces mediating collisions. Investigations of proton transfer reaction mechanisms are important for understanding such fundamental biological, physical, and chemical processes as solvation, photosynthesis, acid-base neutralization, and enzymatic reactions.<sup>3,4</sup> Light particle transfer between two heavier functional groups is governed both by kinematic and dynamical constraints, and studies in the gas phase have the potential to distinguish the roles of these distinct factors. Conventional treatments of charge transfer reactions often consider the processes as occurring at long range, with little momentum transfer between the approaching reactants or the separating products.<sup>5</sup> Such long-range encounters raise questions about the role of energy resonance and Franck-Condon factors in effecting electron transfer.<sup>6</sup> However, the possibility that electron transfer may be coupled to particle transfer suggests that motions over an extended range of internuclear separations may also play an important role in the dynamics of such processes. Systems

that undergo charge transfer as well as hydrogen/deuterium isotope exchange provide important examples of encounters in which electron transfer may occur in regions of the potential energy surface where all atoms in the collision system interact strongly. Among the specific systems that may undergo these processes, the reactions of water cations with hydrocarbons are relevant to many basic natural and industrial processes. The  $H_2O^+$  ion and its deuterated analogs are well-known reactive species that are present in interstellar clouds,<sup>7,8</sup> combustion processes,<sup>9,10</sup> and chemical ionization mass spectrometry.<sup>11</sup> Ethylene is known as a component of circumstellar shells<sup>7,8</sup> and plays an important role in combustion processes of hydrocarbon fuels.<sup>9</sup>

In this paper, we present crossed beam studies of charge transfer between  $D_2O^+$  and  $C_2H_4$  in which simple electron transfer to form  $C_2H_4^+$  via reaction (1), or rearrangement charge transfer to form  $C_2H_3D^+$  by reaction (2) can occur. In addition, deuterium ion transfer to form  $C_2H_4D^+$  via reaction (3) can also be observed



The charge transfer reaction is exothermic with  $\Delta H$

<sup>a)</sup>Electronic mail: farrar@chem.rochester.edu

= -2.11 eV (-203.6 kJ/mole); the deuterium ion transfer reaction is also exothermic, with  $\Delta H = -0.91$  eV (-87.8 kJ/mole).

The reactions of  $\text{H}_2\text{O}^+$  and  $\text{D}_2\text{O}^+ + \text{C}_2\text{H}_4$  have been studied previously both experimentally and theoretically by several groups. One of the earliest studies, by Rakshit and Warneck,<sup>12</sup> employed a drift chamber mass spectrometer to determine products and rate coefficients of charge transfer reactions. Dotan and coworkers<sup>13</sup> measured the total rate constant for the reaction of ionized water with ethylene in a flow-drift tube. Fishman and Grabowski<sup>14</sup> also measured rate coefficients using a selected ion flow tube. None of the studies employing  $\text{D}_2\text{O}^+$  reported the occurrence of charge transfer with H/D exchange. Theoretically, density functional theory (DFT) calculations to determine the mechanisms and structures of intermediates were performed by Qu *et al.*<sup>15</sup> By measuring product flux distributions in conjunction with DFT calculations on the structures of possible intermediate complexes, the present work provides significant insight into the dynamics of the charge transfer processes.

## II. EXPERIMENT

The experimental apparatus has been described previously,<sup>16</sup> so only a brief review is made here.  $\text{D}_2\text{O}^+$  ions are produced by electron impact on deuterium oxide vapor. The measured pressure in the initial focusing stage vacuum chamber is about  $8 \times 10^{-5}$  Torr; from conductance estimates, we believe the pressure in the ionization volume is approximately 0.01 Torr. The ions are accelerated to 300 V, and the desired ions are then mass-selected with a  $60^\circ$  magnetic sector. After deceleration to the desired beam energy and focusing by a series of ion optics, the beam has an energy distribution with a full width at half maximum of  $\sim 0.20$  to 0.45 eV. Experiments were performed at selected energies over a relative collision energy range of 0.28 to 0.79 eV (27.0 to 76.2 kJ/mole). The ethylene beam is formed by supersonic expansion of the pure gas through a 0.07 mm nozzle. A 1.0 mm diameter skimmer located 50 nozzle diameters downstream from the nozzle selects the cool core of the beam. Before entering the main chamber, the beam is collimated by passing through a 3.0 mm square aperture located approximately 2.5 cm from the skimmer in a differential pumping chamber. In the main chamber, the neutral beam intersects the ion beam at a  $90^\circ$  angle. A tuning fork chopper modulates the neutral beam at 30 Hz, allowing separation of background from the true reactive scattering signal. An electrostatic energy analyzer with resolution of 0.07 eV is used to measure the kinetic energies of ions in the primary ion beam and scattered ionic reaction products. The energy analyzer was calibrated before and after the experiments by measuring the kinetic energy distribution of thermal ions formed by resonant charge transfer between  $\text{He}^+$  and He. The product ions were mass-selected by a quadrupole mass spectrometer and detected by a dual microchannel plate ion detector. Data acquisition was computer controlled.

Two independent measurements were performed in the experiment. The kinetic energy distributions of the scattered product ions were measured at 22 fixed laboratory angles. Each energy spectrum consisted of 80 points, with typical

energy bin widths of 0.025 eV. These kinetic energy distributions were then normalized by measuring angular distributions of product ions in the laboratory coordinate system by summing the signal over all energies. The branching fractions for reactions (1)–(3) were also measured at each collision energy.

## III. DATA ANALYSIS

Dynamical interpretation of the scattering data obtained for reactions (1)–(3) is facilitated by transformation of the kinetic energy and angular distributions of reaction products to the center of mass (c.m.) coordinate system. The reactant beams in the experiments have velocity and angular spreads, resulting in distributions of collision energies and intersection angles. These dispersions must be taken into account when transforming the laboratory data to c.m. coordinates. An iterative deconvolution procedure is used to extract the c.m. cross section from the laboratory flux distributions by inverting the following equation:<sup>17</sup>

$$I_{\text{lab}}(v, \Theta) = \sum_{i=1}^N f_i \frac{v^2}{u_i^2} I_{\text{c.m.}}(u_i, \theta_i). \quad (4)$$

In this expression,  $v$  and  $u_i$  are the velocities in the laboratory and c.m. coordinates, respectively, and  $f_i$  is the weighing factor for Newton diagram  $i$  based on the reagent beam distributions. The extracted  $I_{\text{c.m.}}(u, \theta)$  can be transformed back to the lab frame, allowing comparison between the results of the deconvolution and the experimental data. Five points are used to represent the energy distributions of each of the reagent beams, and five points represent the intersection angle distribution; thus, in the above equation,  $N$  is 125. Application of this deconvolution procedure produces c.m. cross sections  $I_{\text{c.m.}}(u, \theta)$ , that when transformed back to the laboratory with appropriate averaging over experimental velocity distributions and beam intersection angles, recover the experimental data with a standard deviation of  $\leq 14\%$ .

The barycentric angular distributions  $g(\theta)$  of the products are calculated by integrating the derived  $I_{\text{c.m.}}(u, \theta)$  over product translational energy.<sup>18</sup> The function  $g(\theta)$  represents the relative intensities of products scattered into c.m. scattering angle  $\theta$  averaged over product kinetic energy, evaluated by integration over c.m. speed  $u$ , as indicated in Eq. (5)

$$g(\theta) = \int_0^\infty I_{\text{c.m.}}(u, \theta) du. \quad (5)$$

Similarly, the angle-averaged relative translational energy distribution of products,  $P(E_T')$ , are calculated by integrating the c.m. intensity over angle, as follows:

$$P(E_T') = \int_0^\pi u^{-1} I_{\text{c.m.}}(u, \theta) \sin \theta d\theta. \quad (6)$$

The full flux distributions in velocity space as well as the kinetic energy and angular distributions derived from them provide important physical insight into the nature of reactive collisions.

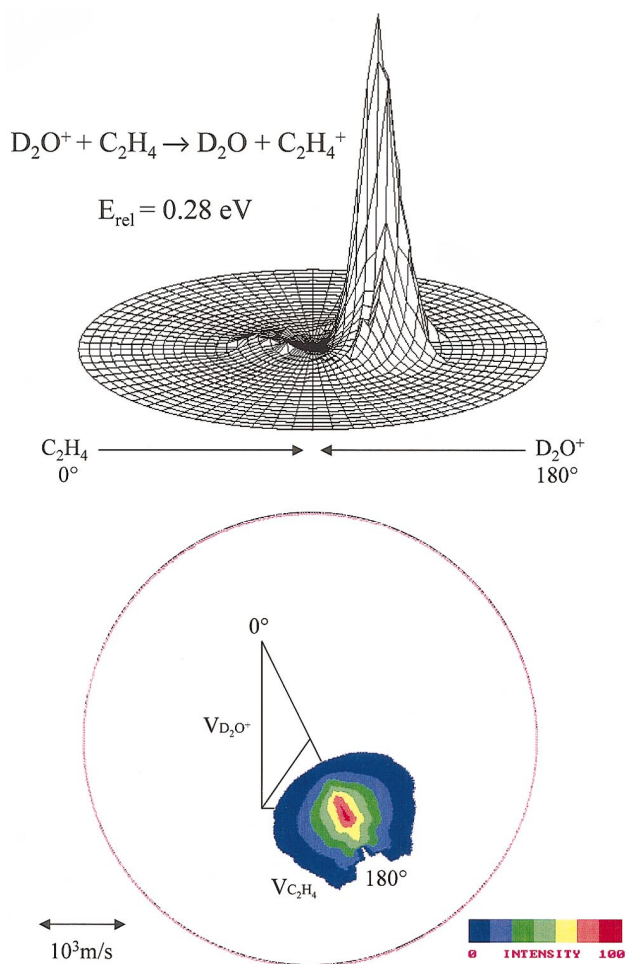


FIG. 1. (Color) Top panel: axonometric representation of the  $C_2H_4^+$  product flux in velocity space from  $D_2O^+ + C_2H_4$  charge transfer, 0.28 eV. Bottom panel: contour plot representation of  $C_2H_4^+$  product flux superimposed on Newton diagram. Circle on contour map defines maximum  $C_2H_4^+$  product velocity allowed by energy conservation.

## IV. RESULTS

### A. Direct charge transfer: $D_2O^+ + C_2H_4 \rightarrow D_2O + C_2H_4^+$

The experiments were carried out at relative collision energies of 0.28, 0.55, and 0.79 eV (27.0, 53.1, and 76.2 kJ/mole). The flux distributions in c.m. coordinates for the  $C_2H_4^+$  products were obtained by iterative deconvolution at all three collision energies. Figure 1 shows the flux distribution for the  $C_2H_4^+$  products at the lowest collision energy. The top panel of the figure shows an axonometric representation of the flux and the lower panel shows a contour projection of the distribution superimposed on the Newton kinematic diagram. In the c.m. coordinate system, the directions of the  $D_2O^+$  ion beam and the  $C_2H_4$  neutral beam are  $0^\circ$  and  $180^\circ$ , respectively. The three bit resolution of the scale of the contour plots provides a qualitative picture of the dynamics; the greater resolution of the axonometric representation is useful for viewing weak features in the presence of more intense flux components. The distributions at the higher collision energies are qualitatively similar to those in Fig. 1 and are not shown here.

The experimental results shown in the flux map indicate

that the charge transfer flux distribution is sharply asymmetric, with the majority of the  $C_2H_4^+$  products scattered in the same direction as the precursor beam, with product velocities similar to the reagent neutral beam velocities. Because of the convention that the parent ion beam defines the  $0^\circ$  direction in c.m. coordinates, the charge transfer products are assigned to the angular range near  $180^\circ$ . Normally, this direction is denoted *backward*; however, in reaction systems in which the charged products originate from the neutral reagent, this nomenclature is confusing. For the present discussion, we adopt the convention that products formed with momenta similar in direction and magnitude to their precursor reactants are considered *forward* scattered. In the context of the charge transfer products  $C_2H_4^+/C_2H_3D^+$ , the observation of forward-scattered products indicates that the dominant charge transfer reaction mechanism is direct. The axonometric plot in Fig. 1 shows that there is a small component of flux in the backward hemisphere, consistent with participation of a complex that lives a small fraction of a rotational period. The nature of such a complex is discussed in a later section of this paper.

The angular distributions and relative translational energy distributions of the products of the charge transfer reaction at all three energies are shown in Fig. 2. At the lowest collision energy, the angular distribution has a width appreciably larger than at the higher collision energies. The small, but perceptible peak in the backward direction correlates with the weak feature we noted in the axonometric plot of Fig. 1. Figure 2(b) shows the relative translational energy distributions of the product at the three energies. As the collision energy increases, the translational energy distributions of the products shift toward higher energies and increase in width. At the higher collision energies, the kinetic energy distributions show partially resolved structure that may be associated with the production of specific vibrational energy levels of the products. However, the large number of product vibrational modes precludes an assignment of these features.

The energy disposal results for the charge transfer process to form  $C_2H_4^+$  are summarized in Table I. The total energy is the sum of collision energy  $E_{rel}$ , any reactant internal energy, and the reaction exothermicity. Under the high pressure operating conditions of the ion source, electronic excitation should be quenched,<sup>19</sup> and partial vibrational relaxation should be achieved. As discussed below, experimental results are consistent with total energies accessible to these collision systems in which reactants have no significant vibrational energy. The supersonic expansion produces internally cold neutral reactants. The product relative energy  $E_T'$  at each collision energy is tabulated as the average value of the appropriate relative translational energy distribution in Fig. 2(b). From conservation of energy, we determine that the fraction of the total energy appearing in product translation increases from 14 to 22% as the collision energy spans the full range studied here. Table I shows that the average internal excitation of the reaction products is 2.06 eV (199 kJ/mole) at the lowest collision energy, identical to the reaction exothermicity of 2.11 eV (203.6 kJ/mole) within experimental error. With increasing collision energy, the average product internal excitation increases to 2.28 eV (220.0 kJ/

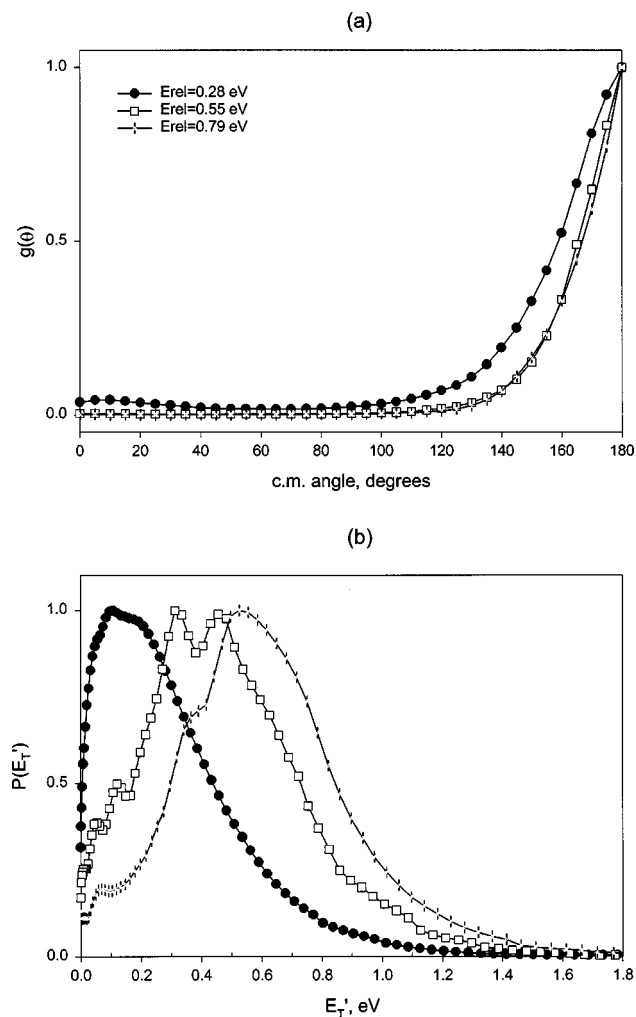


FIG. 2. (a) Angular distributions for  $C_2H_4^+$  charge transfer products, all energies. (b) kinetic energy distributions for  $C_2H_4^+$  charge transfer products, all energies.

mole) at the highest collision energy, demonstrating that a small fraction of the incremental incident translational energy is transformed into product internal excitation.

### B. Charge transfer with H/D exchange: $D_2O^+ + C_2H_4 \rightarrow HOD + C_2H_3D^+$

Charge transfer with rearrangement was studied by detecting the mass 29 product. In Fig. 3, we show the polar flux distribution for  $C_2H_3D^+$  formation at the lowest collision energy. The major feature of this polar flux distribution is similar both qualitatively and quantitatively to that shown in Fig. 1 for the direct charge transfer reaction. The distribu-

TABLE I. Reaction energy partitioning results for  $D_2O^+ + C_2H_4 \rightarrow D_2O + C_2H_4^+$  (units in eV).

Ion energy	0.39	0.85	1.26
Reactant relative energy, $E_{rel}$	0.28	0.55	0.79
Total energy, $E_{total}$	2.39	2.66	2.90
Product average relative energy, $\langle E_T' \rangle$	0.32	0.50	0.62
$\langle E_T' \rangle / E_{total}$	14%	19%	22%
Product average internal energy	2.06	2.16	2.28

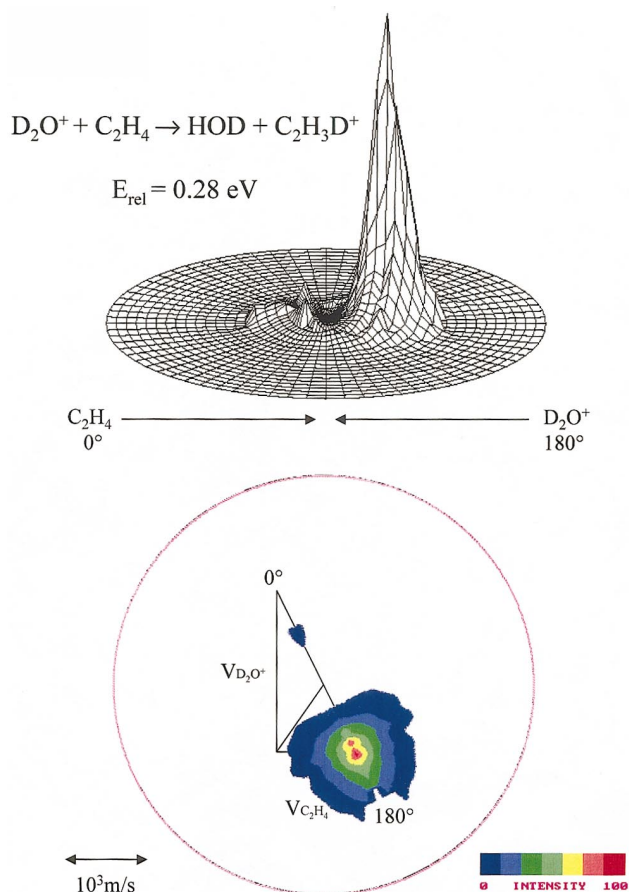


FIG. 3. (Color) Top panel: axonometric representation of the  $C_2H_3D^+$  rearrangement charge transfer product flux in velocity space from  $D_2O^+ + C_2H_4$  charge transfer, 0.28 eV. Bottom panel: contour plot representation of  $C_2H_3D^+$  product flux superimposed on Newton diagram. Circle on contour map defines maximum  $C_2H_3D^+$  product velocity allowed by energy conservation.

tions at the two higher collision energies are similar to that shown in Fig. 3. As in the direct reaction channel, the flux distributions for  $C_2H_3D^+$  formation are asymmetric, with maxima near the precursor ethylene beam.

Figure 3 shows that the  $C_2H_3D^+$  flux distribution has a significant component of backward scattering at the lowest collision energy, which is a factor of three to four more intense than the corresponding feature in the  $C_2H_4^+$  product distribution in Fig. 1. This backward scattering component diminishes with increasing collision energy. That conclusion is reinforced by the appearance of the product angular distributions plotted in the top panel of Fig. 4. While the angular distributions are primarily peaked near the ethylene beam at  $180^\circ$ , i.e., they correspond to forward scattered products, there is significant backward scattering, especially at the lowest collision energy. Such scattering likely arises from small impact parameter collisions, the fraction of which appears to be enhanced at lower collision energies, an observation consistent with the participation of a transient intermediate complex.

For each energy, the c.m. translational energy distributions are shown in the lower panel of Fig. 4, with numerical results summarized in Table II. The kinetic energy distribu-

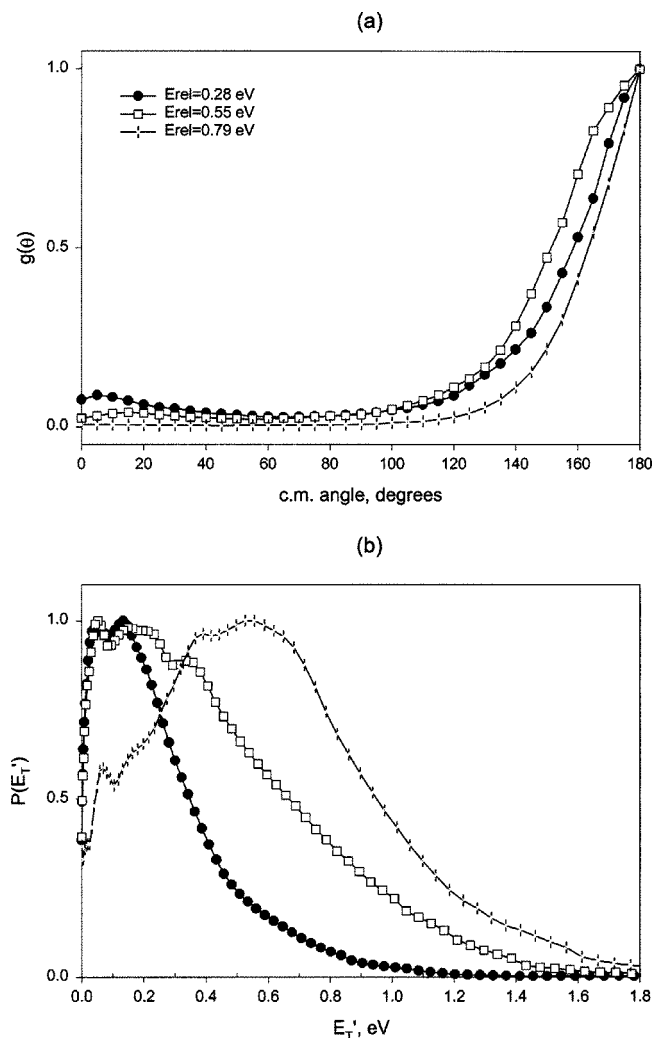


FIG. 4. (a) Angular distributions for  $C_2H_3D^+$  rearrangement charge transfer products, all energies. (b) Kinetic energy distributions for  $C_2H_3D^+$  rearrangement charge transfer products, all energies.

tions for charge transfer with rearrangement are qualitatively similar to those for direct charge transfer in that they broaden and shift with increasing collision energy. The results show that the average internal energies of reaction products increase only slightly with increasing collision energy.

### C. Deuterium ion transfer: $D_2O^+ + C_2H_4 \rightarrow OD + C_2H_4D^+$

The deuterium ion transfer reaction was studied at c.m. collision energies of 0.34, 0.55, and 0.78 eV (32.8, 53.1, and 75.2 kJ/mole). The flux distribution of  $C_2H_4D^+$  products at a collision energy of 0.34 eV is shown in Fig. 5. The distribu-

TABLE II. Reaction energy partitioning results for  $D_2O^+ + C_2H_4 \rightarrow HOD + C_2H_3D^+$  (units in eV).

Ion energy	0.39	0.85	1.26
Reactant relative energy, $E_{rel}$	0.28	0.55	0.79
Total energy, $E_{total}$	2.39	2.66	2.90
Product average relative energy, $\langle E_T' \rangle$	0.29	0.47	0.63
$\langle E_T' \rangle / E_{total}$	12%	18%	22%
Product average internal energy	2.10	2.19	2.27

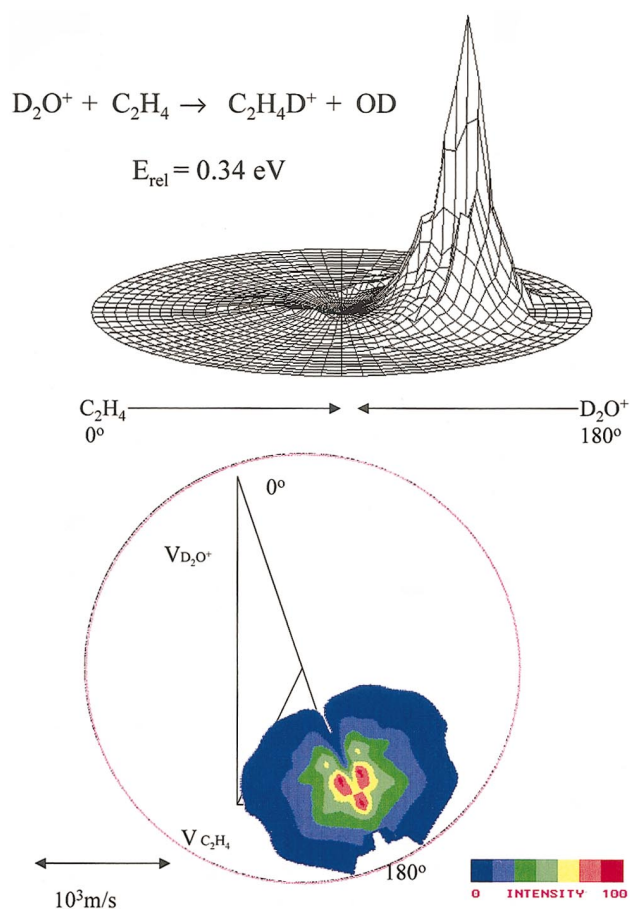


FIG. 5. (Color) Top panel: axonometric representation of the  $C_2H_4D^+$  product flux in velocity space from reaction of  $D_2O^+$  and  $C_2H_4$ , 0.34 eV. Bottom panel: contour plot representation of  $C_2H_4D^+$  product flux superimposed on Newton diagram.

tions at higher collision energies are qualitatively similar to those at lower collision energy, and are not shown. The flux plot shown in Fig. 5 presents contours of constant product flux in c.m. velocity space, and shows that the products appear in the same region of velocity space as the incident ethylene beam, indicating that they are forward scattered. There is a very small component of backward scattering at the lowest collision energy, indicative of reaction from small impact parameters. The strong forward scattering continues to higher collision energies, and indicates that the deuterium ion transfer reaction is direct, proceeding on a time scale much shorter than a rotational period of the transient association complex of the approaching reactants. This impulsive behavior is typical of dynamics of exothermic proton (deuteron) transfer reactions.

The top panel of Fig. 6 shows the product angular distributions at all three collision energies as obtained from Eq. (5). All of the product angular distributions are peaked near  $180^\circ$ , defined by convention as the direction of the neutral  $C_2H_4$  beam. As previously noted, the reaction products are considered forward scattered, since their momenta are strongly correlated with those of the precursor reactants. The widths of the angular distributions show a slight narrowing with increasing collision energy, consistent with decreased interaction times at higher kinetic energies.

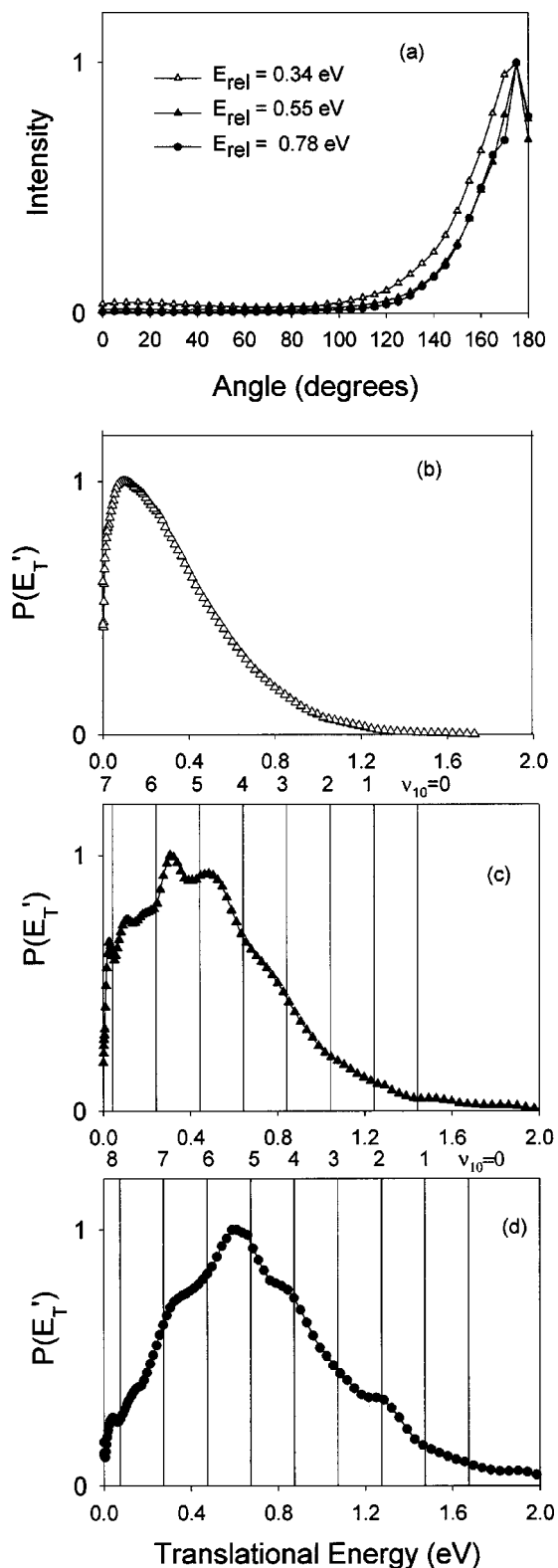


FIG. 6. (a) Angular distributions for  $C_2H_4D^+$  deuterium ion transfer products, all energies. (b)–(d) Product relative kinetic energy distributions for  $C_2H_4D^+$  formation, all energies. Vertical lines in panels (c) and (d) correspond to product velocity corresponding to specified quanta in  $\nu_{10}$  mode of  $C_2H_4D^+$  product formed with internally cold OD.

The lower panels of Fig. 6 show that the product kinetic energy distributions exhibit a systematic shift toward higher product translational energies with increasing collision en-

TABLE III. Reaction energy partitioning results for  $D_2O^+ + C_2H_4 \rightarrow OD + C_2H_4D^+$  (units in eV).

	0.49	0.84	1.24
Ion energy	0.49	0.84	1.24
Reactant relative energy, $E_{rel}$	0.34	0.55	0.78
Total energy, $E_{total}$	1.25	1.46	1.69
Product average relative energy, $\langle E_T' \rangle$	0.36	0.53	0.74
$\langle E_T' \rangle / E_{total}$	29%	36%	44%
Product average internal energy	0.89	0.93	0.95

ergy. At the lowest collision energy, the products exhibit a sharp peak at low translational energy with a tail that extends to the thermochemical limit. The most probable product kinetic energy is below 0.1 eV, and the mean energy of the distribution occurs at 0.36 eV, corresponding to 29% of the available energy in product translation. The mean product internal energy is 0.89 eV, essentially identical to the reaction exothermicity.

At the next collision energy 0.55 eV, the distribution has shifted to higher translational energies, and reproducible structure appears in the distribution. The mean product translational energy has shifted upward to 0.53 eV; the mean internal excitation of the reaction products is 0.93 eV, still equal to the reaction exothermicity within experimental error. At the highest collision energy of 0.78 eV, the product translational energy distribution has again shifted upward, the mean energy increasing to 0.74 eV. The mean product internal energy is 0.95 eV, again equal to the reaction exothermicity within experimental error. The structure that was first observed at 0.55 eV collision energy persists at this energy. At the fixed total energy of these experiments, selective population of product vibrational modes in conjunction with favorable kinematics and minimal rotational excitation will create periodic structures in the kinetic energy distributions. We will discuss the possible origin of such structures in the next section.

The energy partitioning results are summarized in Table III. The data show a number of interesting trends. First, the mean product internal excitation is constant and equal to the reaction exothermicity within  $\pm 4\%$ . Second, the partitioning of the *incremental* translational energies in the two highest energy experiments is particularly illuminating. In the 0.55 eV experiment, the 0.21 eV increment in reactant translational energy relative to the lowest energy experiment appears primarily in incremental translation. On the average, 0.17 eV of this 0.21 eV increment, or 81%, appears in product translation. The effect is even more pronounced at the highest collision energy, where, of the 0.23 eV increase in reactant translation, 0.21 eV or 91% appears in product translation. As we will discuss later, the preferential partitioning of incremental reactant translation into product translation is characteristic of light particle transfer between two heavier molecular fragments.

#### D. Product branching ratios

Careful measurements of the relative intensities of the products of reactions (1)–(3) were obtained at all three collision energies. Independent of collision energy, deuterium ion transfer accounts for approximately 20% of the reactive

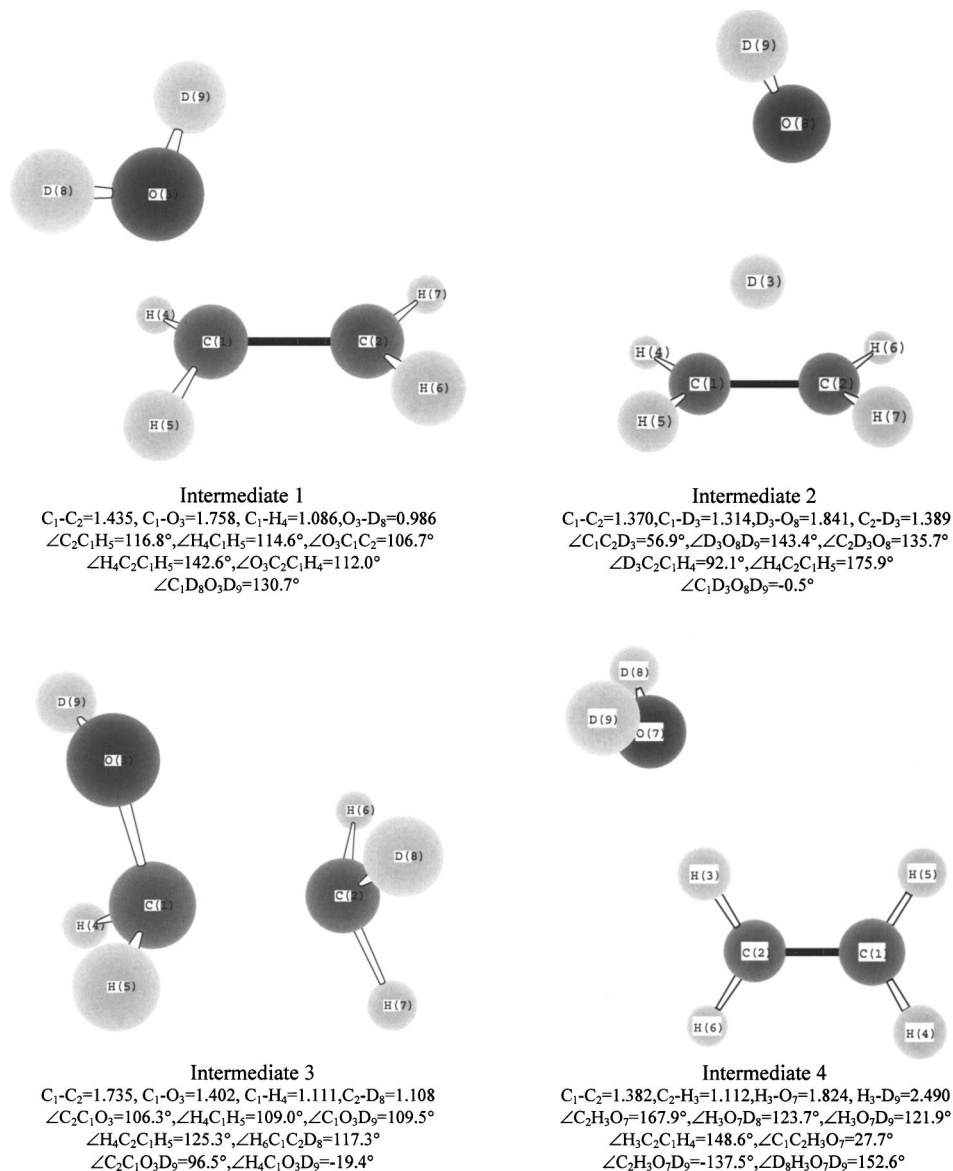


FIG. 7. Geometries of intermediates and transition states from DFT calculations, described in text. Below each species, the bond lengths (in Å) and angles are indicated.

collisions. The remainder of the reactive processes were assigned to charge transfer. The isotopic labeling allowed us to distinguish direct charge transfer to form  $C_2H_4^+$  from collisions in which H/D exchange formed  $C_2H_3D^+$  products. The rearrangement channel was most important at the lowest collision energy, where 36% of the charge transfer collisions occur with rearrangement. That fraction decreased monotonically to 22% at the highest energy. The fact that the cross section for rearrangement charge transfer is comparable in magnitude to direct charge transfer will play an important role in understanding the pathways for reaction.

## V. DFT CALCULATIONS

We also performed DFT calculations with the GAUSSIAN 98 program package<sup>20</sup> in order to elucidate structures of important reactive intermediates and the transition states connecting them. The geometries of all the relevant species were fully optimized at the B3LYP/6-311+G\* level, and com-

plex vibrational frequencies were then extracted in the harmonic approximation. The frequencies of the deuterated species were calculated by replacing hydrogen with deuterium at corresponding sites. Single point energy calculations were performed at the B3LYP/6-311+G\* and B3LYP/6-311++G\*\* levels of theory based on the B3LYP/6-311+G\* geometries and zero-point vibrational energies. From the calculations, for all the open shell species  $S^2$ , the spin-squared expectations are close to the ideal value of 0.75 for spin eigenstates, indicating that spin contamination may be ignored. With minor exceptions, the calculations reproduce those reported by Qu *et al.*<sup>15</sup>

The calculations show that two important intermediates play a direct role in the formation of  $C_2H_4^+$ . The DFT calculations indicate that in these intermediates, the positive charge is on  $C_2H_4$ . The first bound species on the reaction coordinate, denoted structure 1 in Fig. 7, corresponds to a complex of ethylene cation with neutral  $D_2O$  electrostatically

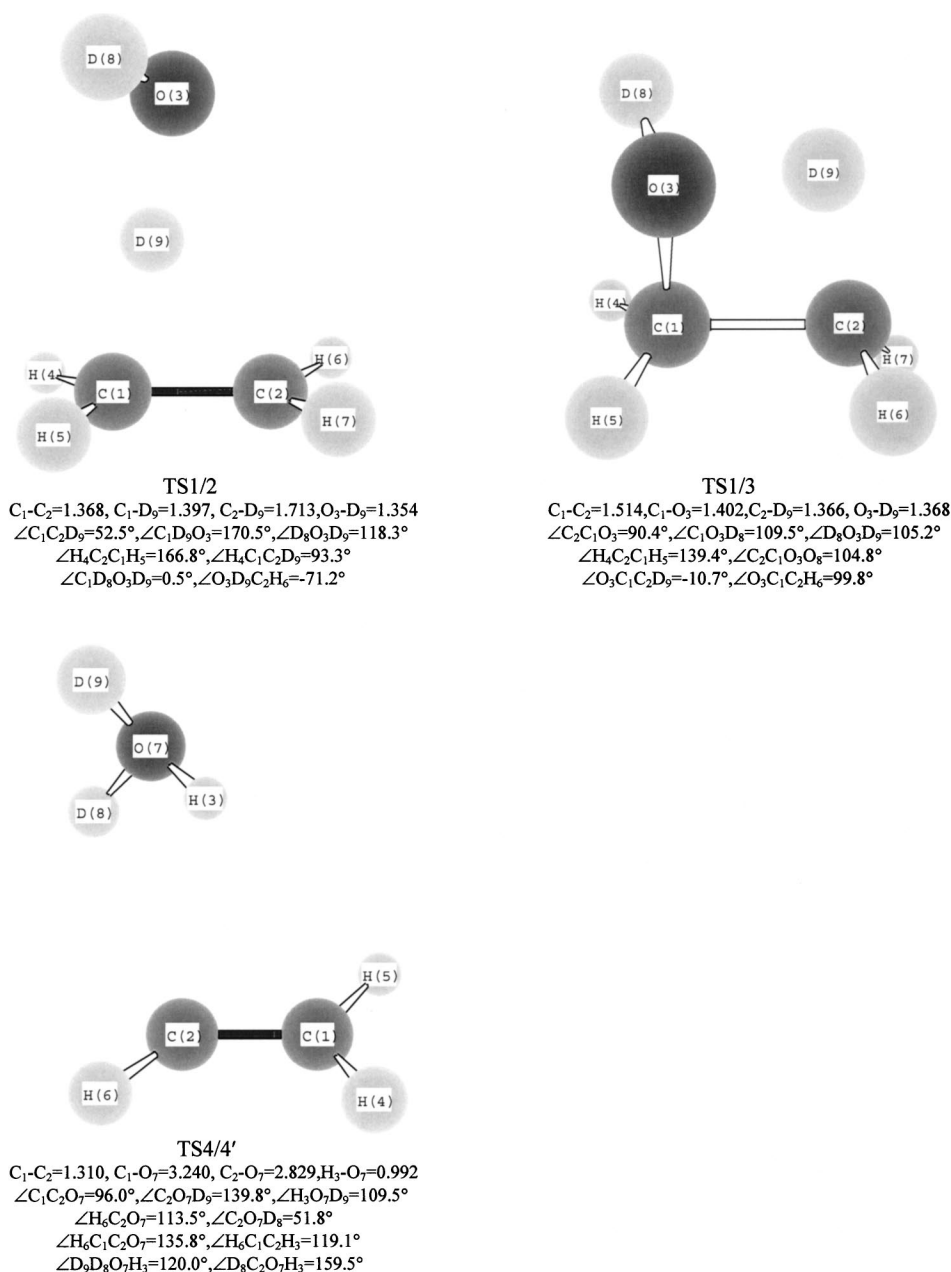


FIG. 7. (Continued.)

bound along the  $C \cdots O$  coordinate. This complex is stable with respect to reactants by 3.17 eV (306 kJ/mole). The identification of complex 1 as the first bound species on the reaction coordinate indicates that electron transfer from  $C_2H_4$  to  $D_2O^+$  occurs at long range while the reactants are approaching. A second electrostatically bound complex that consists of an ethylene cation bound to  $D_2O$ , but in a hydrogen bonded-like  $O \cdots H-C$  configuration, denoted in Fig. 7 as structure 4, is also accessed by the approaching reactants. This species, which is bound by 2.91 eV (281 kJ/mole), also decays to the charge transfer products without a barrier in excess of the endothermicity.

A bound intermediate, denoted structure 2 in Fig. 7, is formed when one of the D atoms in  $D_2O^+$  approaches the  $\pi$ -electron cloud on ethylene along the C-C perpendicular bisector. This complex is characterized by incipient deute-

rium ion transfer, ultimately yielding the bridged ethyl cation and an OD radical by simple bond cleavage.

The calculations also suggest the existence of a fourth intermediate, structure 3 in Fig. 7, that is formed when complex 1 isomerizes via a four-center transition state to an isomer of ethanol cation in which the C-C bond is significantly elongated relative to its equilibrium geometry. If complex 3 is accessed, its lowest energy decay channel, as reported by Qu *et al.*,<sup>15</sup> is via C-C bond cleavage to produce  $CH_2OH^+ + CH_2D$ . The absence of any ions at  $m/e=31$  suggests that this intermediate does not play an important role in the reaction dynamics.

Complexes 1, 2, and 4 appear to serve as direct precursors for the products of direct charge transfer and deuterium ion transfer, decaying by simple bond cleavages without barriers in excess of their endothermicities. However, hydrogen/

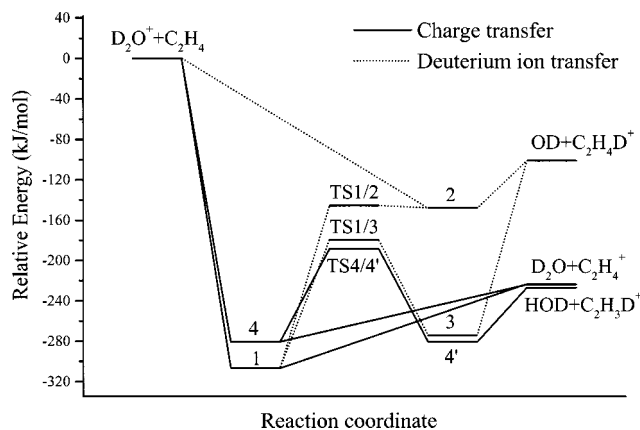


FIG. 8. Schematic reaction coordinate for direct and rearrangement charge transfer and deuterium ion transfer. Solid lines indicate pathways for charge transfer through complexes 1 and 4. Dashed lines indicate pathways for deuterium ion transfer. The charge transfer channels are linked to the deuterium ion transfer process via complexes 2 and 3, as described in the text.

deuterium migrations in these complexes allow them to interconvert, providing additional pathways to form  $C_2H_4D^+$  by  $D^+$  transfer as well as charge transfer with rearrangement to form  $C_2H_3D^+ + HOD$ . We also applied DFT calculations to understand these pathways for isomerization. First, we sought pathways that allow exchange of hydrogen and deuterium atoms. The electrostatic complex 4 may exchange hydrogen/deuterium atoms through a bridging transition state  $TS4/4'$ , followed by decay to the products of charge transfer with rearrangement. We also discovered an isomerization pathway that couples the charge transfer and deuterium ion transfer channels: structure 1 may isomerize to complex 2 through an internal rotation of the  $D_2O^+$  moiety that moves a D-atom toward the  $\pi$ -cloud of the ethylene molecule. The transition state for this process is denoted  $TS1/2$ .

The reaction coordinate diagram of Fig. 8 summarizes the reaction paths accessible to this system. The DFT calculations allow us to evaluate vibrational frequencies for bound complexes and for transition states, which can be used as input into rate constant calculations using Rice-Ramsperger-Kassel-Marcus (RRKM) statistical theory.<sup>21–24</sup> By examining the relative rate constants for direct dissociation in comparison with isomerization, we may discover additional constraints on reactive pathways.

We first consider the rate constants for direct decay of complexes 1, 2, and 4. Complexes 1 and 4 may serve as precursors to  $C_2H_4^+$  formation by direct charge transfer, and complex 2 is an intermediate for deuterium ion transfer. Frequencies for the transition states were determined for structures in which the bond representing the reaction coordinate is extended to 4.5 Å.<sup>25</sup> The calculations show that simple decay of complexes 1 and 4 to the charge transfer products occurs with rates of  $5 \times 10^{14}$  and  $7 \times 10^{13} \text{ s}^{-1}$ , respectively. The calculations show that decay of complex 2 to  $C_2H_4D^+$  products occurs with a rate of approximately  $5 \times 10^{13} \text{ s}^{-1}$ . These rates are significantly higher than the rotational, and some vibrational, frequencies of the complexes, as estimated from their moments of inertia and total angular momenta. The rates indicate that any complexes that are formed are too

short-lived to behave statistically, and are therefore consistent with the direct dynamics we observe for these processes.

The charge transfer with rearrangement channel clearly requires H/D exchange, and the most likely pathway for this process occurs through hydrogen atom migration via transition state  $TS4/4'$ . The RRKM rate for this migration is estimated to be  $3 \times 10^{10} \text{ s}^{-1}$ , a factor of 2000 slower than direct charge transfer via complex 4. The statistical prediction for the fraction of charge transfer products that occur with rearrangement is therefore  $5 \times 10^{-4}$ . The observed fraction lies in the range between 0.22 and 0.36, the fraction increasing with decreasing collision energy. The large disparity between the experimental data and the predictions of statistical rate theory show very clearly that charge transfer with H/D exchange is a highly nonstatistical process. The chemical reaction takes place through selective molecular motions that are significantly more efficient than ergodic sampling of all accessible phase space.

## VI. DISCUSSION

The experimental data in concert with DFT calculations suggest that the product branching is governed in large part by the relative orientations of approaching reactants. When the  $D_2O^+$  reactant approach is directed principally toward a carbon atom, or along a trajectory that proceeds through a nearly collinear  $O \cdots H-C$  geometry, then the electrostatic complexes 1 or 4 will be formed and charge transfer will follow. Trajectories in which one of the incoming O–D bonds is directed toward the  $\pi$ -electron cloud along the perpendicular bisector of the C–C bond lead toward complex 2 and ultimately to the products of deuterium ion transfer.

The experimental data on direct charge transfer to form  $C_2H_4^+$  indicate that the dominant contribution to reaction comes from direct processes in which the electron appears to be transferred at long range, with minimal momentum transfer between approaching reactants. Despite the fact that H/D exchange must occur in order to form  $C_2H_3D^+$ , the general characteristics of the flux distributions for this product are very similar to those for the direct charge transfer process. Consequently, our discussion of charge transfer will focus first on the similarities of the two processes. Given the separation of time scales for electron transfer relative to nuclear motion, it is conventional to think of charge transfer from the perspective of processes that do not interconvert translational and internal energy. The importance of Franck-Condon factors and energy resonance on the magnitude of charge transfer rate constants has not been determined definitively, and experimental results suggest that both may contribute to the same reaction.<sup>6</sup> The fact that the mean translational energies of reactants and products are only separated by  $\sim 0.1 \text{ eV}$  at most indicates the importance of energy resonance in these systems. Charge transfer processes may also be allowed even in the absence of resonance between reactant and product ion states, if there is favorable overlap between the wave functions of initial and final electronic-vibrational states. If a charge transfer reaction is allowed by favorable Franck-Condon factors, the transition may occur at large internuclear separations. Namely, charge transfer is a fast process that

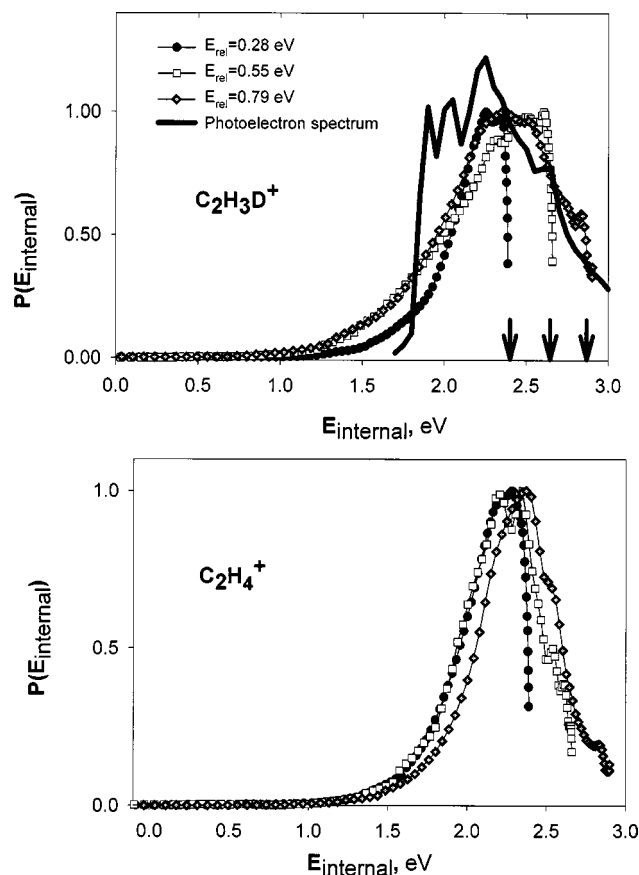


FIG. 9. Internal energy distributions of reaction products for the  $C_2H_3D^+$  products (upper panel), and  $C_2H_4^+$  (lower panel) inferred from product translational energy distributions. The vertical arrows indicate the thermochemical limits for the three different collision energies. The solid curve in the upper panel shows the photoelectron band for formation of  $C_2H_4^+$  ( $C_2H_3D^+$ ) in the first excited  $1^2B_{2g}$  state.

takes place at large ion-molecule separations and on a time scale short compared to nuclear motion.<sup>5</sup>

Experimental work on the photoelectron spectrum of  $C_2H_4$  provides useful information on the nature of the Franck-Condon envelope for formation of  $C_2H_4^+$ .<sup>26</sup> If charge transfer to form  $C_2H_4^+$  is influenced by Franck-Condon factors for ionization of  $C_2H_4$ , then a comparison of the *internal* energy distribution of reaction products with the photoelectron spectrum of  $C_2H_4$  may be instructive. In Fig. 9, we plot the internal energy distributions, computed from the measured translational energy distributions as

$$P_{\text{internal}}(E') = P_{\text{trans}}(E_{\text{total}} - E') \quad (7)$$

for  $C_2H_3D^+$  and  $C_2H_4^+$ . First, we notice that the internal energy distributions of both sets of reaction products are very similar, peaking at high internal energies and cutting off abruptly at the thermochemical limits. The production of ground state  $C_2H_4^+$  by charge transfer from  $D_2O^+$  requires significant interconversion of translational and internal energy, and is therefore suppressed by the lack of energy resonance. However, the second photoelectron band, producing  $C_2H_4^+$  in the  $1^2B_{2g}$  excited state is energy resonant and also has large Franck-Condon factors. Figure 9 shows that the positions and widths of the internal energy distributions of

the reaction products are very similar to the Franck-Condon profile. Although equating the product internal energy distributions with those of  $C_2H_4^+$  ( $C_2H_3D^+$ ) requires the accompanying  $D_2O$  ( $HOD$ ) products to be internally cold, the structural similarities of  $D_2O$  and  $D_2O^+$  are consistent with that hypothesis. With that assumption, the comparison of internal energy distributions with the photoelectron spectrum indicates that the reaction product distributions are governed by Franck-Condon factors and the available energy. As the collision energy increases, the product internal energy distribution appears to follow the Franck-Condon profile, but is limited by energy conservation.

Although the bulk of the experimental data on charge transfer are consistent with direct dynamics constrained by energy resonance and favorable Franck-Condon factors, there are a few features of the data that are inconsistent with this simple picture. Most surprising is the fact that charge transfer with rearrangement, which requires H/D exchange, likely through the agency of an intermediate complex, appears remarkably like direct charge transfer. We have already commented that the likely pathway for H/D exchange involves isomerization of complex 4 through TS 4/4', but that the statistical rate for this process is three orders of magnitude smaller than observed; i.e., the statistical mechanism produces negligible  $C_2H_3D^+$ . Nevertheless, an examination of the subtleties of the experimental data appears to support the limited participation of one or more intermediate complexes in the charge transfer process. In particular, the formation of  $C_2H_3D^+$  at the lowest collision energy has a significant component of backward scattering, shown directly in the axonometric plot of Fig. 3 and also in the angular distributions of Fig. 4. The data are consistent with a few percent of the reactive flux proceeding through an intermediate complex.

A simple kinetic analysis gives us some bounds. If complex 4 decays in parallel to two different products, the branching ratio for the two products is given by the ratio of rate constants. Treating the backward scattered products as coming from isomerizing complex 4, their intensity suggests that the rate for this process is a few percent of the rate for direct decay of complex 4. This would imply that the actual rate for isomerization of complex 4 is of magnitude  $10^{12} \text{ s}^{-1}$ , which is comparable to the rotation rate of the complex, but still significantly faster than the statistical rate. The experimental data thus suggest that a small fraction of the  $C_2H_3D^+$  products are formed in a manner consistent with limited participation of a transient complex that decays non-statistically. However, the majority of these products are produced on a time scale inconsistent with this pathway and appear to proceed as direct reactions. In like manner, the data also suggest that an even smaller fraction of the  $C_2H_4^+$  products are formed through an intermediate. Additional theoretical work will help illuminate the nature of such processes.

A similar argument may hold for the formation of  $C_2H_4D^+$  products. As we already noted, the charge transfer and deuterium ion transfer processes may be coupled via isomerization of complex 1 through transition state TS 1/2. RRKM calculations predict that the rate of isomerization along the  $1 \rightarrow 2$  pathway is  $3 \times 10^{10} \text{ s}^{-1}$ , approximately three

orders of magnitude slower than decay of complex 2 to  $C_2H_4D^+$ . If  $C_2H_4D^+$  can be produced via two parallel routes, i.e., through complex 2, or through rate-limiting isomerization via the  $1 \rightarrow 2$  pathway, then experimental differentiation between these two sets of products gives the ratio of rate constants for the parallel pathways. Products passing through TS1/2 are formed on a time scale longer than a rotational period of either complex, and will therefore have a flux distribution symmetric about  $\pi/2$  in the c.m. system. The experimental data of Fig. 5 demonstrate that products formed through these different routes may be distinguished through their angular distributions: The strong forward peak is attributed to  $C_2H_4D^+$  produced via direct reaction, and the small contribution to the reactive flux in the backward direction provides evidence that a small fraction of the products are formed with a rate slow on the timescale of intermediate complex rotation.

We estimate that the backward scattered contribution accounts for no more than one percent of the reactive flux. The kinetic argument for parallel channels suggests that decay through the isomerization route occurs at a rate in the low  $10^{12} \text{ s}^{-1}$  regime. This value is well above the statistical prediction, and may suggest that the  $1 \rightarrow 2$  isomerization pathway is sampled nonstatistically. The contribution from the isomerization path to the forward-scattered flux will be hidden under the low energy rising edge of the direct flux. However, we cannot discount the possibility that low impact parameter collisions generate a small yield of backward scattered products through a direct mechanism. Simulations of reactive trajectories may illuminate this issue.

Like the charge transfer processes, the deuterium ion transfer channel also creates highly internally excited products. The discussion of energy partitioning in the deuterium ion transfer process first begins by establishing the *baseline* partitioning of energy at a fixed reference energy. The data at the lowest collision energy show that 71% of the available energy is partitioned in product internal excitation. The product translational energy distribution does not provide any detailed information concerning the manner in which this energy is partitioned between products, or into specific modes of motion. However, the quantitative transformation of the entire reaction exothermicity into internal excitation is consistent with an early release of the exothermicity with the nascent bond extended from its equilibrium configuration. Like previous work from this laboratory<sup>27</sup> on proton transfer from  $H_3O^+$  to  $NH_3$ , the present system demonstrates very similar behavior, suggestive of particle transfer in which the incipient bond is highly extended from its equilibrium geometry.

Both the  $H_3O^+ + NH_3$  and  $D_2O^+ + C_2H_4$  proton/deuterium ion transfer reactions are examples of a Heavy + Light-Heavy system in which a light particle, i.e., H or D, is transferred between heavier molecular fragments. Kinematics play an important role in particle transfer reactions with this particular mass combination. The potential energy surface for this transfer, expressed in the scaled and skewed coordinates that remove cross terms in the kinetic energy quadratic form<sup>28</sup> is characterized by a very acute angle,  $24^\circ$  for this system, between the entrance and exit channels. At

low collision energies, the classic energy disposal motif for this mass combination is that of “mixed energy release” in which the new bond is formed in an extended configuration, as the old bond cleaves simultaneously. The extensive trajectory studies of Anlauf *et al.*,<sup>29,30</sup> Maylotte, Polanyi, and Woodall,<sup>31</sup> and Parr, Polanyi, and Wong<sup>32</sup> show that reactive collisions on such highly skewed surfaces are direct, with a strong propensity to cut the corner separating the entrance and exit valleys. These motions correspond to light atom transfer from configurations extended from equilibrium bond lengths with little momentum transfer to the departing heavy atoms, yielding reaction products that are highly vibrationally excited. The high degree of internal excitation observed in the  $C_2H_4D^+$  and OD products is consistent with mixed energy release.

More detailed insight into the reactive dynamics comes from the experimental data at the higher collision energies. First, the product kinetic energy distributions at 0.55 and 0.78 eV shift toward higher energies in such a way as to preserve the complete transformation of reaction exothermicity into product internal excitation on the average. This observation is consistent with the mixed energy release picture of particle transfer, in which the nascent bond is formed in an extended position. Second, both kinetic energy distributions show oscillations at regular spacings that provide additional dynamical information. The vertical lines in the plots of the translational energy distributions at 0.55 and 0.78 eV in Fig. 6(b) correspond to the kinetic energies of rotationally cold species in which the  $C_2H_4D^+$  product has a specified number of quanta in the  $\nu_{10}$  vibration. This vibration corresponds to motion of the bridging D atom perpendicular to the C–C bond framework. DFT calculations predict a frequency of  $1530 \text{ cm}^{-1}$ , which yields a spacing of 0.19 eV in the kinetic energy distribution. Rotational excitation in either fragment accounts for the shifts in the observed peak positions relative to the calculated positions. The spacings of the oscillatory components are sufficiently similar to those predicted for excitation of the  $\nu_{10}$  mode as to suggest a strong correlation. This correlation is strengthened by the role that complex 2 plays in the deuterium ion transfer reaction, facilitating the formation of the bridged ethyl cation with the transferred D atom significantly displaced from its equilibrium configuration. This Franck-Condon-like picture is analogous to the interpretation of energy release in the  $O^- + CH_4$  system, in which the nascent  $CH_3$  radical arises from a transition state in which the local geometry about the carbon atom is tetrahedral, leading to excitation of the umbrella mode in the  $CH_3$  product.<sup>33</sup>

The small skew angle of the reduced dimensionality surface that describes deuteron transfer provides an explanation for the transformation of incremental translational energy into product translation. The concept of “induced repulsive energy release” was introduced by Ding *et al.* to address partitioning of incremental translational energy on Heavy + Light-Heavy potential surfaces.<sup>34</sup> In this picture, reactive trajectories with excess translation penetrate far into the “corner” of the highly skewed potential surface where both the forming and breaking bonds are compressed. The trajectory moves into the exit valley with little motion perpendicu-

lar to the reaction coordinate, yielding products with high translational excitation. Depending on the extent to which the collision geometry in the corner is bent, the nascent products will partition some of the incident translation into product rotation. The trajectory therefore explores a new portion of the potential surface relative to reference trajectories at lower energies. The corner cutting trajectories that produce vibrationally excited products at lower collision energies are replaced by trajectories at higher translational energy that are more effective at reaching the compressed configurations that facilitate translation in the separating products. Consistent with our observations, “induced repulsive energy release” predicts that channeling of reactant translation into product translation is more effective at higher collision energies.

## VII. CONCLUSIONS

The crossed beam experiments and supporting DFT calculations reported in this paper provide a very high resolution view of the reactive dynamics of the charge transfer and deuterium ion transfer reactions of  $D_2O^+ + C_2H_4$ . The work has elucidated key features of the potential energy surfaces mediating the reactions and the nature of reactive motion on those surfaces. The calculations suggest that the approach geometry of the ion relative to the carbon framework controls the reactive pathways. Approach of  $D_2O^+$  toward a carbon atom or toward a C–H bond in a near-collinear  $O \cdots H-C$  configuration leads to the formation of electrostatically bound complexes that decay to the products of charge transfer. In contrast, the approach of  $D_2O^+$  such that a deuterium atom is oriented toward the  $\pi$ -electron cloud of ethylene along the perpendicular bisector of the C–C bond leads to a complex in which  $D^+$  transfer proceeds smoothly to form the bridged ethyl cation. To lowest order, simple models for reaction describe the collision processes: Charge transfer is driven by favorable Franck-Condon factors for producing  $C_2H_4^+$  in the energy-resonant  $1^2B_{2g}$  excited state. The deuterium ion transfer process is direct, and proceeds through the familiar mixed energy transfer motif, in which both the forming and breaking bonds are extended. A long progression in the  $\nu_{10}$  mode of the ethyl cation provides elegant confirmation of this picture.

However, a number of subtle surprises also accompany the results. There are distinct contributions from backward scattered products in all reactive processes, particularly at the lowest collision energies. The role of small impact parameter collisions and transient collision complexes in yielding such products requires additional theoretical interpretation. In addition, energy disposal and product angular distributions in the direct charge transfer process forming  $C_2H_4^+ + D_2O$  are virtually identical to those for charge transfer with H/D exchange to form  $C_2H_3D^+ + HOD$ . Apparently the reactive dynamics are determined in large part by long-range electron transfer, and subsequent H/D exchange interactions at shorter range that are required in the  $C_2H_3D^+$  pathway provide only small modifications of the nascent Franck-Condon distribution. Equally surprising is the fact that  $C_2H_3D^+$  production is a factor of  $10^3$  larger than predicted by the statistical

isomerization rates describing H/D exchange. Evidently, there exists a very specific pathway for H/D exchange that is much more efficient than ergodic exploration of the entire phase space accessible to products. These questions require calculations of the reactive dynamics on potential energy surfaces that model the key coordinates for charge and deuterium ion transfer realistically. Such calculations will be computationally challenging. We hope the present work will stimulate such studies.

## ACKNOWLEDGMENT

We gratefully acknowledge the U.S. Department of Energy for financial support.

- <sup>1</sup> *Gas Phase Ion Chemistry*, Vol. 1, 2, edited by M. T. Bowers (Academic, New York, 1979).
- <sup>2</sup> *Ionic Processes in the Gas Phase*, edited by M. A. Almoester Ferreira (D. Reidel, Dordrecht, Holland, 1984).
- <sup>3</sup> *Proton Transfer Reactions*, edited by E. Caldin and V. Gold (Chapman and Hall, London, 1975).
- <sup>4</sup> M. Rini, B.-Z. Magnes, E. Pines, and E. T. J. Nibbering, *Science* **301**, 349 (2003).
- <sup>5</sup> P. M. Hierl, V. Pacak, and Z. Herman, *J. Chem. Phys.* **67**, 2678 (1977).
- <sup>6</sup> M. T. Bowers and D. D. Elleman, *Chem. Phys. Lett.* **16**, 486 (1972).
- <sup>7</sup> D. Smith, *Chem. Rev. (Washington, D.C.)* **92**, 1473 (1992).
- <sup>8</sup> D. Smith and P. Spänel, *Mass Spectrom. Rev.* **14**, 255 (1995).
- <sup>9</sup> D. J. Hucknall, *Chemistry of Hydrocarbon Combustion* (Chapman and Hall, London, 1985).
- <sup>10</sup> S. D. Tanner, J. M. Goodings, and D. K. Bohme, *Can. J. Chem.* **59**, 1760 (1981).
- <sup>11</sup> A. G. Harrison, *Chemical Ionization Mass Spectrometry*, 2nd ed. (CRC, Boca Raton, 1992).
- <sup>12</sup> A. B. Rakshit and P. Warneck, *J. Chem. Soc., Faraday Trans. 2* **76**, 1084 (1980).
- <sup>13</sup> I. Dotan, W. Lindinger, B. Rowe, D. W. Fahey, F. C. Fehsenfeld, and D. L. Albritton, *Chem. Phys. Lett.* **72**, 67 (1980).
- <sup>14</sup> V. N. Fishman and J. J. Grabowski, *J. Phys. Chem. A* **103**, 4879 (1999).
- <sup>15</sup> Z.-w. Qu, H. Zhu, X.-k. Zhang, and Q.-y. Zhang, *Chem. Phys. Lett.* **354**, 498 (2002).
- <sup>16</sup> D. F. Varley, D. J. Levandier, and J. M. Farrar, *J. Chem. Phys.* **96**, 8806 (1992).
- <sup>17</sup> P. E. Siska, *J. Chem. Phys.* **59**, 6052 (1973).
- <sup>18</sup> Z. Herman, *Int. J. Mass. Spectrom.* **212**, 413 (2001).
- <sup>19</sup> J. E. Moryl, W. R. Creasy, and J. M. Farrar, *J. Chem. Phys.* **82**, 2244 (1985).
- <sup>20</sup> M. J. Frisch, G. W. Trucks, H. B. Schlegel *et al.*, GAUSSIAN 98, Revision A.11.1, Gaussian, Inc., Pittsburgh, PA, 2001.
- <sup>21</sup> T. Baer and W. L. Hase, *Unimolecular Reaction Dynamics: Theory and Experiments* (Oxford University Press, New York, 1996).
- <sup>22</sup> L. S. Kassel, *J. Phys. Chem.* **32**, 225 (1928).
- <sup>23</sup> R. A. Marcus and O. K. Rice, *J. Phys. Colloid Chem.* **55**, 894 (1951).
- <sup>24</sup> O. K. Rice and H. C. Ramsperger, *J. Am. Chem. Soc.* **49**, 1617 (1927).
- <sup>25</sup> Y. Li and T. Baer, *J. Phys. Chem. A* **106**, 8658 (2002).
- <sup>26</sup> K. Kimura, S. Katsumata, Y. Achiba, T. Yamazaki, and S. Iwata, *Handbook of He I Photoelectron Spectra of Fundamental Organic Molecules* (Halsted, New York, 1980).
- <sup>27</sup> Y. Li and J. M. Farrar, *J. Chem. Phys.* **120**, 199 (2004).
- <sup>28</sup> J. O. Hirschfelder, *Int. J. Quantum Chem., Symp.* **3**, 17 (1969).
- <sup>29</sup> K. G. Anlauf, P. J. Kuntz, D. H. Maylotte, P. D. Pacey, and J. C. Polanyi, *Discuss. Faraday Soc.* **44**, 183 (1967).
- <sup>30</sup> K. G. Anlauf, J. C. Polanyi, W. H. Wong, and K. B. Woodall, *J. Chem. Phys.* **49**, 5189 (1968).
- <sup>31</sup> D. H. Maylotte, J. C. Polanyi, and K. B. Woodall, *J. Chem. Phys.* **57**, 1547 (1972).
- <sup>32</sup> C. A. Parr, J. C. Polanyi, and W. H. Wong, *J. Chem. Phys.* **58**, 5 (1973).
- <sup>33</sup> M. A. Carpenter and J. M. Farrar, *J. Chem. Phys.* **106**, 5951 (1997).
- <sup>34</sup> A. M. G. Ding, L. J. Kirsch, D. S. Perry, J. C. Polanyi, and J. L. Schreiber, *Faraday Discuss. Chem. Soc.* **55**, 252 (1973).